Ultra-long-range symmetric plasmonic waveguide for high-density and compact photonic devices

Chia-Chien Huang*

Department of Physics and Institute of Nanoscience, National Chung Hsing University, Taichung 40227, Taiwan
**cch@phys.nchu.edu.tw*

Abstract: This study reports a symmetric hybrid plasmonic waveguide consisting of a cylindrical metal nanowire surrounded by low-index SiO_2 and high-index Si covered with SiO_2. The symmetric circumambience relative to the metal nanowire significantly facilitates the present design to minimize the energy attenuation resulting from Ohmic losses while retaining highly confined modes guided in the low-index nanoscale gaps between the metal nanowire and the high-index Si. The geometric dependence of the mode characteristics on the proposed structure is analyzed in detail, showing long propagation lengths beyond 10 mm with normalized mode areas on the order of 10^{-2}. In addition to enabling the building of long-range plasmonic circuit interconnects, the compactness and high-density integration of the proposed structure are examined by analyzing crosstalk in a directional coupler composed of two such waveguides and bending losses for a 90° bend. A relatively short coupling length of 1.16 μm is obtained at a center-to-center separation of 0.26 μm between adjacent waveguides. Increasing the separation to 1.65 μm could completely prevent coupling between waveguides. Power transmission exceeds 80% in the case of a 90° bend with small radius of curvature of 0.5 μm. Moreover, the dependence of spectral response on coupling length and the transmission of a 90° bend, ranging from telecom wavelengths of 1.40 to 1.65 μm, are investigated. Over a wide wavelength range, a strong coupling length dependence on wavelength and a high transmission for a 90° bend also make the proposed plasmonic waveguide promising for the realization of wavelength-selective components.

OCIS codes: (130.2790) Guided waves; (130.3120) Integrated optics devices; (240.6680) Surface plasmons; (250.5300) Photonic integrated circuits; (250.5403) Plasmonics.

References and links

1. W. L. Barnes, A. Dereux, and T. W. Ebbesen, "Surface plasmon subwavelength optics," Nature **424**(6950), 824–830 (2003).
2. J. Takahara, S. Yamagishi, H. Taki, A. Morimoto, and T. Kobayashi, "Guiding of a one-dimensional optical beam with nanometer diameter," Opt. Lett. **22**(7), 475–477 (1997).
3. P. Berini, "Plasmon-polariton waves guided by thin lossy metal films of finite width: bound modes of symmetric structures," Phys. Rev. B **61**(15), 10484–10503 (2000).
4. P. Berini, "Plasmon-polariton modes guided by a metal film of finite width bounded by different dielectrics," Opt. Express **7**(10), 329–335 (2000).
5. S. I. Bozhevolnyi, V. S. Volkov, E. Devaux, J. Y. Laluet, and T. W. Ebbesen, "Channel plasmon subwavelength waveguide components including interferometers and ring resonators," Nature **440**(7083), 508–511 (2006).
6. D. F. P. Pile, T. Ogawa, D. K. Gramotnev, T. Okamoto, M. Haraguchi, M. Fukui, and S. Matsuo, "Theoretical and experimental investigation of strongly localized plasmons on triangular metal wedges for subwavelength waveguiding," Appl. Phys. Lett. **87**(6), 061106 (2005).
7. M. Yan and M. Qiu, "Guided plasmon polariton at 2D metal corners," J. Opt. Soc. Am. B **24**(9), 2333–2342 (2007).

#199173 - $15.00 USD Received 8 Oct 2013; revised 18 Nov 2013; accepted 18 Nov 2013; published 21 Nov 2013

8. E. Moreno, S. G. Rodrigo, S. I. Bozhevolnyi, L. Martín-Moreno, and F. J. García-Vidal, "Guiding and focusing of electromagnetic fields with wedge plasmon polaritons," Phys. Rev. Lett. **100**(2), 023901 (2008).
9. G. Veronis and S. H. Fan, "Guided subwavelength plasmonic mode supported by a slot in a thin metal film," Opt. Lett. **30**(24), 3359–3361 (2005).
10. T. Holmgaard and S. I. Bozhevolnyi, "Theoretical analysis of dielectric-loaded surface plasmon polariton waveguides," Phys. Rev. B **75**(24), 245405 (2007).
11. R. F. Oulton, V. J. Sorger, D. A. Genov, D. F. P. Pile, and X. Zhang, "A hybrid plasmonic waveguide for subwavelength confinement and long-range propagation," Nat. Photonics **2**(8), 496–500 (2008).
12. R. F. Oulton, V. J. Sorger, T. Zentgraf, R. M. Ma, C. Gladden, L. Dai, G. Bartal, and X. Zhang, "Plasmon lasers at deep subwavelength scale," Nature **461**(7264), 629–632 (2009).
13. X. D. Yang, Y. Liu, R. F. Oulton, X. B. Yin, and X. Zhang, "Optical forces in hybrid plasmonic waveguides," Nano Lett. **11**(2), 321–328 (2011).
14. V. J. Sorger, Z. Ye, R. F. Oulton, Y. Wang, G. Bartal, X. B. Yin, and X. Zhang, "Experimental demonstration of low-loss optical waveguiding at deep sub-wavelength scales," Nat. Commun. **2**(331), 1–5 (2011).
15. Y. J. Lu, J. S. Kim, H. Y. Chen, C. H. Wu, N. Dabidian, C. E. Sanders, C. Y. Wang, M. Y. Lu, B. H. Li, X. G. Qiu, W. H. Chang, L. J. Chen, G. Shvets, C. K. Shih, and S. G. Gwo, "Plasmonic nanolaser using epitaxially grown silver film," Science **337**(6093), 450–453 (2012).
16. M. Z. Alam, J. Meier, J. S. Aitchison, and M. Mojahedi, "Propagation characteristics of hybrid modes supported by metal-low-high index waveguides and bends," Opt. Express **18**(12), 12971–12979 (2010).
17. D. X. Dai and S. L. He, "Low-loss hybrid plasmonic waveguide with double low-index nano-slots," Opt. Express **18**(17), 17958–17966 (2010).
18. X. L. Zuo and Z. J. Sun, "Low-loss plasmonic hybrid optical ridge waveguide on silicon-on-insulator substrate," Opt. Lett. **36**(15), 2946–2948 (2011).
19. Y. S. Bian, Z. Zheng, Y. Liu, J. S. Liu, J. S. Zhu, and T. Zhou, "Hybrid wedge plasmon polariton waveguide with good fabrication-error-tolerance for ultra-deep-subwavelength mode confinement," Opt. Express **19**(23), 22417–22422 (2011).
20. C. C. Huang, "Hybrid plasmonic waveguide comprising a semiconductor nanowire and metal ridge for low-loss propagation and nanoscale confinement," IEEE J. Sel. Top. Quantum Electron. **18**(6), 1661–1668 (2012).
21. P. F. Yang, Z. G. Di, and H. X. Xu, "Low-loss light transmission in a rectangular-shaped hybrid metal trench at 1550 nm," Opt. Express **21**(14), 17053–17059 (2013).
22. R. Adato and J. P. Guo, "Modification of dispersion, localization, and attenuation of thin metal stripe symmetric surface plasmon-polariton modes by thin dielectric layers," J. Appl. Phys. **105**(3), 034306 (2009).
23. B. F. Yun, G. H. Hu, Y. Ji, and Y. P. Cui, "Characteristics analysis of a hybrid surface plasmonic waveguide with nanometric confinement and high optical intensity," J. Opt. Soc. Am. B **26**(10), 1924–1929 (2009).
24. Y. S. Bian, Z. Zheng, X. Zhao, J. S. Zhu, and T. Zhou, "Symmetric hybrid surface plasmon polariton waveguides for 3D photonic integration," Opt. Express **17**(23), 21320–21325 (2009).
25. T. Holmgaard, J. Gosciniak, and S. I. Bozhevolnyi, "Long-range dielectric-loaded surface plasmon-polariton waveguides," Opt. Express **18**(22), 23009–23015 (2010).
26. Y. Kou, F. W. Ye, and X. F. Chen, "Low-loss hybrid plasmonic waveguide for compact and high-efficient photonic integration," Opt. Express **19**(12), 11746–11752 (2011).
27. L. Chen, X. Li, G. P. Wang, W. Li, S. H. Chen, L. Xiao, and D. S. Gao, "A silicon-based 3-D hybrid long-range plasmonic waveguide for nanophotonic integration," J. Lightwave Technol. **30**(1), 163–168 (2012).
28. Y. S. Bian, Z. Zheng, X. Zhao, Y. L. Su, L. Liu, J. S. Liu, J. S. Zhu, and T. Zhou, "Guiding of long-range hybrid plasmon polariton in a coupled nanowire array at deep-subwavelength scale," IEEE Photon. Technol. Lett. **24**(15), 1279–1281 (2012).
29. L. Chen, T. Zhang, X. Li, and W. P. Huang, "Novel hybrid plasmonic waveguide consisting of two identical dielectric nanowires symmetrically placed on each side of a thin metal film," Opt. Express **20**(18), 20535–20544 (2012).
30. V. S. Volkov, Z. H. Han, M. G. Nielsen, K. Leosson, H. Keshmiri, J. Gosciniak, O. Albrektsen, and S. I. Bozhevolnyi, "Long-range dielectric-loaded surface plasmon polariton waveguides operating at telecommunication wavelengths," Opt. Lett. **36**(21), 4278–4280 (2011).
31. C. Xiang and J. Wang, "Long-range hybrid plasmonic slot waveguide," IEEE Photon. J. **5**(2), 4800311 (2013).
32. V. A. Zenin, Z. H. Han, V. S. Volkov, K. Leosson, I. P. Radko, and S. I. Bozhevolnyi, "Directional coupling in long-range dielectric-loaded plasmonic waveguides," Opt. Express **21**(7), 8799–8807 (2013).
33. X. Guo, M. Qiu, J. Bao, B. J. Wiley, Q. Yang, X. Zhang, Y. Ma, H. Yu, and L. Tong, "Direct coupling of plasmonic and photonic nanowires for hybrid nanophotonic components and circuits," Nano Lett. **9**(12), 4515–4519 (2009).
34. Y. G. Ma, X. Y. Li, H. K. Yu, L. M. Tong, Y. Gu, and Q. H. Gong, "Direct measurement of propagation losses in silver nanowires," Opt. Lett. **35**(8), 1160–1162 (2010).
35. Y. S. Bian and Q. H. Gong, "Low-loss light transport at the subwavelength scale in silicon nano-slot based symmetric hybrid plasmonic waveguiding schemes," Opt. Express **21**(20), 23907–23920 (2013).
36. M. Bass, C. Decusatis, J. Enoch, V. Lakshminarayanan, G. F. Li, C. Macdonald, V. Mahajan, and E. V. Stryland, *Handbook of Optics, Volume IV: Optical Properties of Materials, Nonlinear Optics, Quantum Optics* (McGraw-Hill Professional, 2009).
37. P. B. Johnson and R. W. Christy, "Optical constants of the noble metals," Phys. Rev. B **6**(12), 4370–4379

#199173 - $15.00 USD Received 8 Oct 2013; revised 18 Nov 2013; accepted 18 Nov 2013; published 21 Nov 2013

(1972).
38. S. A. Maier, *Plasmonics: Fundamentals and Applications* (Springer, 2007), Chap. 1.
39. V. R. Almeida, Q. F. Xu, C. A. Barrios, and M. Lipson, "Guiding and confining light in void nanostructure," Opt. Lett. **29**(11), 1209–1211 (2004).
40. R. Buckley and P. Berini, "Figures of merit for 2D surface plasmon waveguides and application to metal stripes," Opt. Express **15**(19), 12174–12182 (2007).
41. C. Y. Jeong, M. Kim, and S. Kim, "Circular hybrid plasmonic waveguide with ultra-long propagation distance," Opt. Express **21**(14), 17404–17412 (2013).
42. S. M. García-Blanco, M. Pollnau, and S. I. Bozhevolnyi, "Loss compensation in long-range dielectric-loaded surface plasmon-polariton waveguides," Opt. Express **19**(25), 25298–25311 (2011).
43. G. Magno, M. Grande, V. Petruzzelli, and A. D'Orazio, "Asymmetric hybrid double dielectric loaded plasmonic waveguides for sensing applications," Sens. Actuators B Chem. **186**(0), 148–155 (2013).
44. K. K. Lee, D. R. Lim, L. C. Kimerling, J. Shin, and F. Cerrina, "Fabrication of ultralow-loss Si/SiO2 waveguides by roughness reduction," Opt. Lett. **26**(23), 1888–1890 (2001).
45. W. P. Huang, "Coupled-mode theory for optical waveguides: an overview," J. Opt. Soc. Am. A. **11**(3), 963–983 (1994)
46. G. Veronis and S. H. Fan, "Crosstalk between three-dimensional plasmonic slot waveguides," Opt. Express **16**(3), 2129–2140 (2008).
47. W. P. Huang, C. Xu, S. T. Chu, and S. K. Chaudhuri, "The finite-difference vector beam propagation method: analysis and assessment," J. Lightwave Technol. **10**(3), 295–305 (1992).
48. A. V. Krasavin and A. V. Zayats, "Three-dimensional numerical modeling of photonic integration with dielectric-loaded SPP waveguides," Phys. Rev. B **78**(4), 045425 (2008).
49. D. Dai and S. He, "A silicon-based hybrid plasmonic waveguide with a metal cap for a nano-scale light confinement," Opt. Express **17**(19), 16646–16653 (2009).
50. A. Amirhosseini and R. Safian, "A hybrid plasmonic waveguide for the propagation of surface plasmon polariton at 1.55 μm on SOI substrate," IEEE Trans. NanoTechnol. **12**(6), 1031–1036 (2013).
51. V. R. Chinni, T. C. Huang, P. K. A. Wai, C. R. Menyuk, and G. J. Simonis, "Crosstalk in a lossy directional coupler switch," J. Lightwave Technol. **13**(7), 1530–1535 (1995).
52. P. Berini and J. J. Lu, "Curved long-range surface plasmon-polariton waveguides," Opt. Express **14**(6), 2365–2371 (2006).
53. M. Z. Alam, J. Meier, J. S. Aitchison, and M. Mojahedi, "Propagation characteristics of hybrid modes supported by metal-low-high index waveguides and bends," Opt. Express **18**(12), 12971–12979 (2010).

1. Introduction

Integrating the areas of nanoelectronic and photonic devices is hindered by the inherent diffraction limit of light energy supported in dielectric media. To circumvent this difficulty, the surface plasmon polariton (SPP) modes excited by coupling an electromagnetic wave to the free-electron collective oscillations at the dielectric-metal interface provide a promising approach to squeeze light into nanoscale regions smaller than the wavelength of light [1]. Therefore, various SPP-based waveguides (or plasmonic waveguides), such as metallic cylinders embedded in dielectrics [2], metal strips [3,4], V-grooves in metal surfaces [5], metal wedges [6–8], and metal slots [9], have been reported in recent years. Nevertheless, the unavoidable problem of using plasmonic waveguides is the huge amount of metallic attenuation leading to short propagation distances. Various waveguide structures [3,4,6–8] support the so-called long-range (LR) SPP modes propagating relatively long distances for efficient plasmonic circuit interconnects but show weak confinement, compared to conventional dielectric waveguides, making them unsuitable for application in high-density integrated photonic circuits. In contrast, the structures [2,5,9] support deep subwavelength modes but short propagation distances (a few micrometers) because of more mode distribution penetrating the metal. To optimize mode confinement and propagation length, the dielectric-loaded SPP waveguide (DLSPPW) [10], that confines mode profiles within the high-index dielectric-loaded media, provides both subwavelength localization and longer propagation distance (a few tens of micrometers). To improve the figure of merit (FOM) for mode confinement and energy loss, Oulton *et al*. [11] proposed a novel hybrid plasmonic waveguide (HPW) comprising a high-index dielectric nanowire separated from a metal surface by a low-index dielectric with nanoscale thickness. Most of the mode energy of the HPW is concentrated in a low-index nanoscale gap dielectric, leading to deep subwavelength confinement and lower loss than that of the DLSPPW where the mode energy is concentrated

#199173 - $15.00 USD Received 8 Oct 2013; revised 18 Nov 2013; accepted 18 Nov 2013; published 21 Nov 2013

in a high-index dielectric. After the pioneering paper [11], the HPW concept has attracted much attention and is widely used to design diverse plasmonic components [12–21]. However, these designs are mainly used for attaining deep subwavelength mode areas on the order of 10^{-2} ($\lambda^2/4$) to 10^{-3} ($\lambda^2/4$), where λ is vacuum wavelength; however, the propagation lengths are limited to tens to several hundreds of micrometers.

On the other hand, achieving long-range signal transportation is definitely indispensable and of practical interest for the realization of large-scale photonic circuit interconnects. As a result, a number of plasmonic waveguide structures [22–32] have been reported to combine the millimeter-scale propagation [3] from the LRSPP with the subwavelength mode confinement [11] from the HPW. Most of these studies [12–32] were mainly aimed at analyzing mode confinements and propagation lengths. Only a few papers [17,24,26,32] addressed the integration problems by analyzing the coupling length of directional couplers. In this study, we propose a new symmetric HPW (SHPW) consisting of a cylindrical metal nanowire bounded from inner to outer regions by low-index silica (SiO_2) and high-index silicon (Si) covered with SiO_2. The propagation lengths of the proposed SHPW are one order of magnitude larger than those reported in [22–32] while maintaining the same order of mode area, 10^{-2} ($\lambda^2/4$). In addition, we study the coupling strength of a directional coupler and the bending loss of a 90° bend by completely examining the compactness and integration of the proposed SHPW, which is applicable for designing various photonic devices. Furthermore, the dependence of the spectral response on the coupling length and the transmission of a 90° bend over a wide range of telecom wavelengths of 1.40 to 1.65 μm are also investigated to evaluate the feasibility of the proposed structure in wavelength-selective components. The remainder of this paper is organized as follows: in Section 2, the geometric dependencies of the proposed SHPW on the essential mode characteristics are described in detail, including mode area, propagation length, and FOM. The crosstalk of a directional coupler composed of two of the proposed HPWs is examined in Section 3. The bending loss of the proposed SHPW along a 90° bend is investigated in Section 4. Finally, the conclusions are presented in Section 5.

2. The geometry dependencies of the proposed SHPW on the mode characteristics

The schematic of the proposed SHPW [Fig. 1(a)] consists of a cylinder metal (Ag) nanowire surrounded by low-index SiO_2 and high-index Si covered by SiO_2. The fabrication processes of the proposed SHPW include some steps. First, we coat a photoresist (PR) thick film (~200 nm) followed by depositing a 2 μm-thick SiO_2 layer on a Si substrate, and then a narrower rectangular groove (to be deposited Si with about 200 nm width and 100 nm height) than the SiO_2 thick film is defined by a patterned hard-mask, a PR exposure with ultraviolet (UV) light and development, and a wet etching process. To form a Si ridge, a Si layer is deposited using chemical vapor deposition (CVD) on the top and then lift off the PR and mask. Next, after coating a PR thin film and a mask, we need to use e-beam lithography to define a rectangular groove (to be deposited SiO_2 film) with several tens of nanometers on the top of the Si ridge. Depositing SiO_2 using molecular beam epitaxy (MBE) on the top because the thickness of the SiO_2 film in this step is needed to be precisely controlled, the groove filled with SiO_2 is formed followed by chemical mechanical polishing (CMP). Removing the mask and PR, two trenches (to be deposited Si) at both sides of the small SiO_2 ridge are formed to be a *W*-type SO_2 geometry. Third, after coating a PR film and using a mask, Si is deposited on top. Removing PR and mask to form two Si ridges (higher than the interior SiO_2 ridge) at both sides of the interior SiO_2. Fourth, coating a PR film and using a mask on the top of the two Si ridges, then an Ag nanowire is put on the interior SiO_2 thin film. Subsequently, we deposit SiO_2 using MBE on the top. Fifth, after removing PR and mask and using CMP to make a flat top surface, we coat a PR film and use a mask to define the groove for depositing Si. After depositing Si and removing PR and mask, the upper part of the Si of the proposed SHPW structure is obtained. Finally, SiO_2 is deposited on the top to finish the proposed SHPW

#199173 - $15.00 USD Received 8 Oct 2013; revised 18 Nov 2013; accepted 18 Nov 2013; published 21 Nov 2013

structure. Regarding with the excitation of the guided mode of the proposed SHPW, the symmetric hybrid guided modes of the proposed structure can be excited by a direct and high-efficiency end-fire coupling using a dielectric slot waveguide with a y-polarized electric field E_y integrated by a tapered optical fiber [33, 34]. The structure of the dielectric slot waveguide adopted here is the same as the present one but without the Ag nanowire [35].

The refractive indices of the SiO_2, Si, and Ag nanowire used in the paper are n_{SiO2} = 1.444, n_{Si} = 3.478 [36], and n_{Ag} = 0.145 – 11.366i [37], respectively, at the telecom wavelength of 1.55 μm. The complex refractive indices of silver taken into account here are from the experimental data [37] and the Drude model [38] fits to the data. The relevant geometric parameters are the diameter of the Ag nanowire, d, the width of the inner SiO_2, w_a, the horizontal gap between the Ag nanowire and the Si, g, and the height and width of the Si, h and w, respectively. The guided mode of the proposed SHPW can be considered as the coupling of the LRSPP mode supported by the metal nanowire [3] and the slot effect due to the large discontinuity of the normal electric field at high-index-contrast interfaces [39]. The numerical results were obtained using the commercial finite-element method (FEM) software COMSOL Multiphysics. To obtain the accurate results, the computational window chosen in COMSOL is 10 μm × 10 μm for avoiding the disturbance from boundary using scattering boundary condition. The maximum and minimum element sizes used in the calculations are 50 nm and 0.5 nm, respectively. The maximum element growth rate is 1.1, the resolution of curvature is 0.3, and the resolution of narrow regions is 4. The high resolution of narrow regions makes the gap be analyzed by enough fineness of mesh to capture the sharp field distribution. For these conditions, the total elements and degrees of freedom are approximately 112932 elements and 792125 unknowns, respectively. For the conditions of w = 200 nm, h = 400 nm, w_a = 100 nm, and d = 10 nm, we observe that the symmetric E_y field profile (y-polarized) is concentrated in the nanoscale gap [Fig. 1(b)] and the longitudinal electric field, $|E_z|$ (responsible for the metal attenuations) is minimized because of the symmetric structure [Fig. 1(c)]. The insets of Figs. 1(b) and 1(c) are the magnified images around the nanowire. Note that the maximum amplitude of the E_y field is two orders of magnitude larger than that of the $|E_z|$ field.

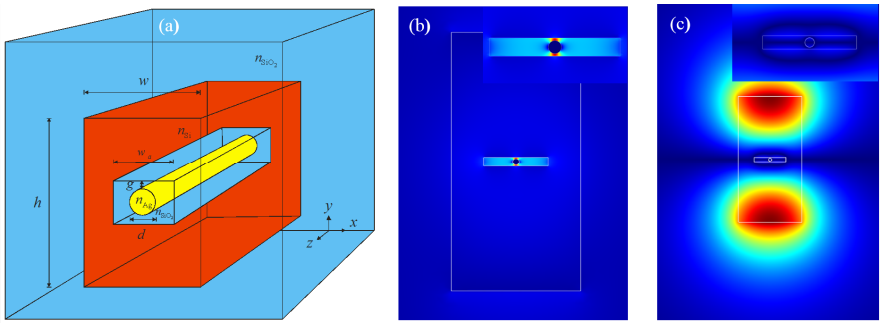

Fig. 1. (a). Schematic of the proposed symmetric hybrid plasmonic waveguide (SHPW) consisting of a cylinder silver (Ag) nanowire surrounded, from the inner to outer media, by low-index SiO_2 and high-index Si covered with SiO_2. (b). The E_y and (c). $|E_z|$ field profiles for dimensions of w = 200 nm, h = 400 nm, w_a = 100 nm, d = 10 nm, and g = 2 nm.

As the gap width g increases, the energy intensity in the gap region is reduced significantly, resulting in less mode confinement due to the weaker coupling between the LRSPP mode and the slot effect. The results are verified by the E_y field distributions of gaps g = 2 nm, 5 nm, and 10 nm shown in Figs. 2(a)–2(c), respectively. For clearly comparing the ability of storing electromagnetic, the energy densities along x = 0 and y = d/2 for different gaps are also shown in Figs. 2(d) and 2(e), respectively. The energy density $W(\mathbf{r})$ is defined as follows:

#199173 - $15.00 USD Received 8 Oct 2013; revised 18 Nov 2013; accepted 18 Nov 2013; published 21 Nov 2013

$$W(\mathbf{r}) = \frac{1}{2}\left\{ \mathrm{Re}\left[\frac{d\varepsilon(\mathbf{r})\omega}{d\omega} \right] |\mathbf{E}(\mathbf{r})|^2 + \mu_0 |\mathbf{H}(\mathbf{r})|^2 \right\}, \quad (1)$$

where ω is the angular frequency, $\varepsilon(\mathbf{r})$ is the profile of relative permittivity, μ_0 is the permeability in vacuum, and $|\mathbf{E}(\mathbf{r})|^2$ and $|\mathbf{H}(\mathbf{r})|^2$ are the electric and magnetic field intensities, respectively. From Figs. 2(d) and 2(e), we observe that decreasing the gap significantly enhances the energy density and obtains smaller mode size.

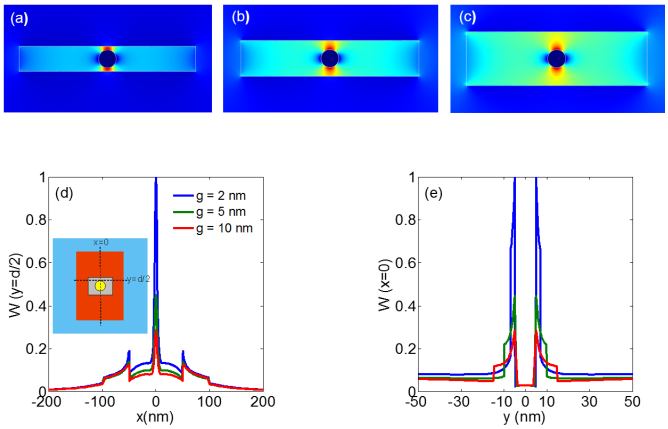

Fig. 2. The E_y field distributions of the proposed SHPW of (a) g = 2 nm, (b) g = 5 nm, and (c) g = 10 nm for dimensions of w = 200 nm, h = 400 nm, w_a = 100 nm, and d = 10 nm. The energy density $W(\mathbf{r})$ along (d) the $y = d/2$ and (e) the x = 0 directions for different gaps.

Accordingly, to achieve better mode confinement, the condition g = 2 nm is fixed throughout the paper. Note that the symmetric x-polarized mode profile concentrated in the vertical gaps can be obtained by altering the aspect ratios of the rectangular geometries of the inner SiO_2 and Si, showing the flexibility of the proposed SHPW to tailor different desired polarizations. To estimate the mode performances of the proposed SHPW, the geometry dependencies on the mode area, propagation length, and FOM proposed by Buckley and Berini in [40] are analyzed in detail. The propagation length is defined as $L_m = \lambda/[4\pi \mathrm{Im}(n_e)]$ indicating the absorption loss, where $\mathrm{Im}(n_e)$ is the imaginary part of the effective mode index n_e. The effective mode area A_e, indicating the mode confinement, is defined as follows:

$$A_e = \frac{W_m}{\max\{W(\mathbf{r})\}} = \frac{1}{\max\{W(\mathbf{r})\}} \int_{-\infty}^{\infty}\int_{\infty}^{\infty} W(\mathbf{r}) d^2\mathbf{r}. \quad (2)$$

The mode area A_e is the ratio of the total mode energy, W_m, to the peak value of the energy density, $W(\mathbf{r})$. Note that the mode area defined in [40] denotes the area surrounded by the closed $1/e$ field magnitude contour relative to the global field maximum. To consistently compare the mode performances with those in other plasmonic structures, the definition of mode area in [40] is replaced by the above mode area, A_e. First, we consider the conditions of w = 200 nm and h = 400 nm. The real part of the effective refractive index, $\mathrm{Re}(n_e)$, the normalized mode area, A_e/A_0, the propagation length, L_m, and the FOM versus the width w_a of the inner SiO_2 are shown in Figs. 3(a)–3(d), respectively, where $A_0 = \lambda^2/4$ denotes the diffraction-limited mode area.

#199173 - $15.00 USD Received 8 Oct 2013; revised 18 Nov 2013; accepted 18 Nov 2013; published 21 Nov 2013

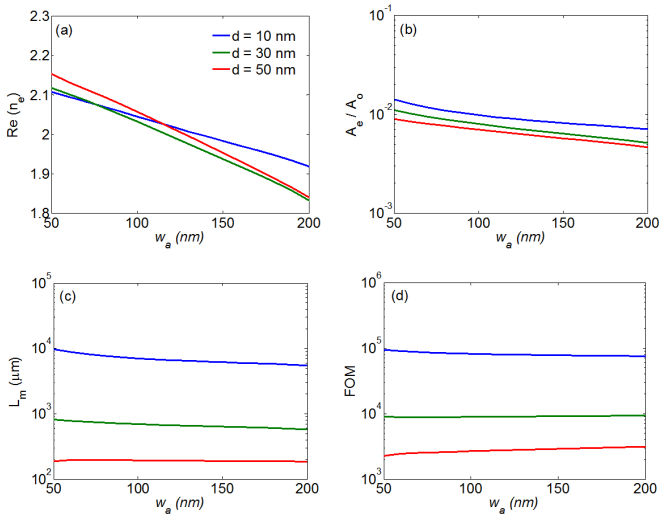

Fig. 3. Mode properties of the proposed SHPW versus the width w_a of the inner SiO_2: (a) real part of the effective refractive index Re(n_e), (b) normalized mode area A_e/A_0, (c) propagation length L_m, (d) figure of merit (FOM), for a gap of g = 2 nm, and Si width of w = 200 nm and height of h = 400 nm, for the three diameters of nanowire shown in Fig. 2(a).

As nanowire diameter increases, we obtain better mode confinement because the coupling of the SPP mode and the slot effect is enhanced and thus results in more energy (major field is E_y) concentrated in the gap. The E_y field distributions of different diameters shown in Figs. 4(a)–4(c) validate this explanation. In contrast, the L_m shows the opposite variation as shown in Fig. 3(c). An increase in nanowire diameter leads to higher absorption loss because of the increase in the penetration of longitudinal electric field $|E_z|$ into the metal nanowire. The mode distributions of $|E_z|$ shown in Figs. 4(d)–4(f) illustrate the phenomenon. For w_a, the Re(n_e) decreases monotonically as w_a increases because some portion of the high-index Si is replaced by the low-index SiO_2. However, the variations of A_e/A_0 and L_m with w_a are slight [Figs. 3(b) and 3(c)] making the FOM almost invariant. This is because the inner SiO_2 is bounded by sufficiently large Si, and therefore the main mode profiles change only within the inner SiO_2 region. From the results, the normalized mode areas of the proposed SHPW are approximately 10^{-2} over a wide range of w_a but the propagation length varies by two orders of magnitude, from 10^2 to 10^4 μm. For d = 10 nm, an L_m of approximately 10 mm can be achieved while retaining the subwavelength mode size, making the proposed SHPW useful for building large-scale and high-density photonic integrated circuits.

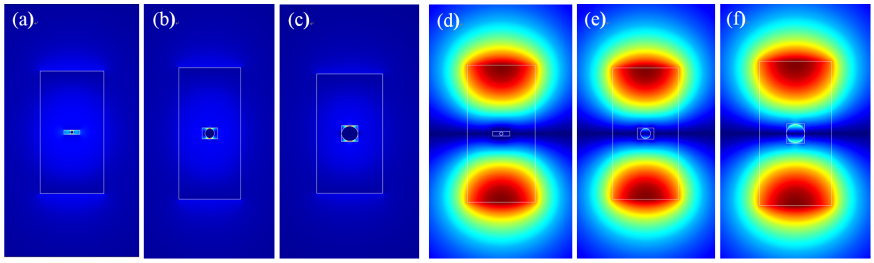

Fig. 4. The E_y distributions of (a) d = 10 nm, (b) d = 30 nm, and (c) d = 50 nm, and the longitudinal electric field $|E_z|$ profiles of (d) d = 10 nm, (e) d = 30 nm, and (f) d = 50 nm, all with dimensions w = 200 nm, h = 400 nm, and w_a = 50 nm.

Next, we consider the geometric effects of the size of Si on the mode characteristics. For different heights of Si, Re(n_e), A_e/A_0, L_m, and FOM versus the width w of Si, with d = 10 nm

#199173 - $15.00 USD Received 8 Oct 2013; revised 18 Nov 2013; accepted 18 Nov 2013; published 21 Nov 2013

and w_a = 100 nm, are shown in Figs. 5(a)–5(d), respectively. As w and h increase, Re(n_e) significantly increases because of the increase in the high-index Si region. Nevertheless, A_e/A_0 and L_m are affected only slightly when w and h exceed 200 nm and 400 nm, respectively. This can be explained by smaller Si causing more energy to spread out of the top and bottom of the Si region, resulting in larger variations in A_e/A_0 and L_m. On the other hand, as we have mentioned above, larger Si reduces the effect of w_a on the mode properties.

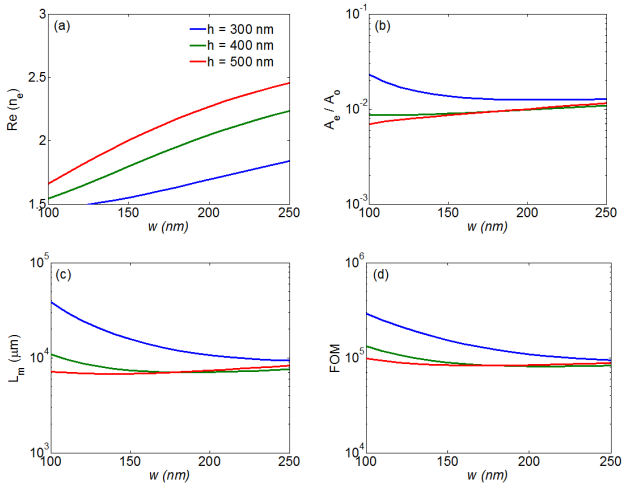

Fig. 5. Mode properties of the proposed SHPW versus the Si width w: (a) real part of the effective refractive index Re(n_e), (b) normalized mode area A_e/A_0, (c) propagation length L_m, (d) figure of merit (FOM), with a gap of g = 2 nm, width of d = 10 nm, and height of w_a = 100 nm, for the three heights of Si shown in Fig. 5(a).

To verify the phenomena, the E_y mode field distributions at w = 100 nm and h = 300 nm with different values of w_a are shown in Figs. 6(a)–6(c) and those at w = 200 nm and h = 400 nm are shown in Figs. 6(d)–6(f). In Fig. 6, we see that larger w_a and the size of Si obtain better mode confinement. Beyond a certain critical size of Si, the variations of mode characteristics are moderate. Note that L_m ≈40 mm can be achieved along with A_e/A_0 ≈0.023 under the conditions of w = 100 nm and h = 300 nm as shown in Figs. 5(b) and 5(c).

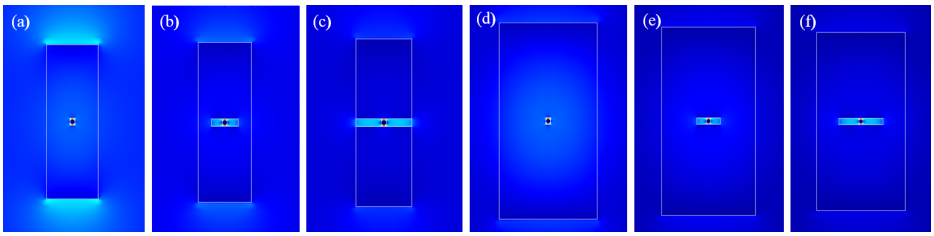

Fig. 6. The E_y distributions of (a) w_a = 10 nm, (b) w_a = 50 nm, and (c) w_a = 100 nm for the dimensions w = 100 nm and h = 300 nm; the E_y distributions of (d) w_a = 10 nm, (e) w_a = 50 nm, and (f) w_a = 100 nm for the dimensions w = 200 nm and h = 400 nm.

To further evaluate the performances of the proposed SHPW, a comparison of mode properties for different HPWs in recent studies is listed in Table 1. For providing a fair comparison, the metals of all the structures are chosen to be silver and the calculations of the mode areas are all based on Eq. (2). In addition, the sizes of high-index Si are comparable. In the proposed SHPW structure, the geometry dimensions used are w = 200 nm, h = 400 nm, w_a = 50 nm, g = 2nm, and d = 20 nm. In [41], the diameter of high-index Si is 400 nm and the cladding is SiO_2. For obtaining the optimal performance in [42], the width and height of ridge of structure 2 are 600 nm and 800 nm, respectively, and the thickness and width of metal strip

#199173 - $15.00 USD Received 8 Oct 2013; revised 18 Nov 2013; accepted 18 Nov 2013; published 21 Nov 2013

are 20 nm and 200 nm, respectively. In [29], the diameters of the two Si wires symmetrically placed on each side of an Ag thin film with thickness of 20 nm are 200 nm and the cladding is SiO_2. The dimensions of the structure LR-SPP hybrid double dielectric-loaded plasmonic waveguide [43] are that the widths and heights of the upper and lower spacers are all 200 nm. The same calculations are also shown for the diameter of Ag, d = 30 nm.

Table 1. Comparison of Mode Properties for Different Hybrid Plasmonic Waveguides

Diameters of metal (Ag)	d = 20 nm			d = 30 nm		
Mode properties	A_e/A_0	L_m (μm)	FOM	A_e/A_0	L_m (μm)	FOM
This proposed SHPW	0.0142	2628.5	25235	0.0110	815.4	8903
Jeong et al. [41]	0.0272	2750.8	19100	0.0209	776.5	6145
Holmgaard et al. [42]	0.2591	5457.7	12269	0.2431	2104.5	4884
Chen et al. [29]	0.0137	356.9	3492	0.0125	155.1	1587
Magno et al. [43]	0.0734	184.6	779	0.0674	85.7	378

From the Table 1, it can be seen that the proposed SHPW possesses the best performance of FOM for different values of d. In [42], the longest propagation length is because that most energy is focused in dielectric ridge. However, the cost paid is the large mode area with wavelength scale. For [29, 43], the higher losses induced are due to the uses of long Ag strips. Particularly, the performances of the circular HPW [41] listed in Table 1 are the second-order mode not the fundamental mode that has extremely high loss. Therefore, avoiding to excite the fundamental mode is another problem for the circular HPW. In summary, the ultra-low-loss SPP modes with subwavelength confinement indeed show the great promise that the proposed SHPW holds for the realization of practical long-range and large-scale photonic integrated circuit interconnects. Regarding with the fabrication imperfections, the device performances affected by the rounded corners of the proposed SHPW are insignificantly. If the sharply right corners of the inner SiO_2 are altered to be rounded corners with maximum radius of curvature of 7 nm, the variations of the normalized mode area A_e/A_0 and the propagation length L_m are smaller than 1.5%. The results of 1.2% are also found in altering the sharp corners of the Si to be rounded corners with radius of curvature of 10 nm. Accordingly, the fabrication imperfection of the proposed SHPW resulted from the corners can be negligible for the device performances because the extremely enhanced field is mainly concentrated in the nanoscale gap not around the corners. Another fabrication imperfections affecting the device performance is the sidewall roughness of dielectrics that increases the scattering losses. Fortunately, the surface roughness of dielectrics can be controlled to be ~2 nm by thermal oxidation method or anisotropic etching [44]. However, the extremely enhanced field in the gap makes the A_e/A_0 and L_m for the gap of g = 4 nm are approximately two times relative to that of the gap of g = 2 nm. Therefore, it will be a major challenge to precisely control the thickness of the gap.

3. The coupling effect of a directional coupler composed of two proposed SHPWs

In addition to having ultra-long-range propagation length (several to tens of millimeters) and subwavelength mode area [$\approx 10^{-2}$ $(\lambda^2/4)$] for a single proposed SHPW, another important factor in the design of high-density plasmonic components is to examine the allowable separation of two adjacent waveguides with negligible crosstalk. As a result, we further analyze the coupling strength of a directional coupler composed of two identical proposed SHPWs. The schematic diagram of the directional coupler is shown in Fig. 7(a), where s is the center-to-center separation distance between the two waveguides. Theoretically, a directional coupler consisting of two single-mode waveguides supports a symmetric (even) and an anti-symmetric (odd) mode relative to the E_y field profiles. For observing mode patterns, we show the E_y fields of even and odd modes in Figs. 7(b) and 7(c), respectively.

#199173 - $15.00 USD Received 8 Oct 2013; revised 18 Nov 2013; accepted 18 Nov 2013; published 21 Nov 2013

Based on the coupled-mode theory (CMT) [45], the coupling strength is gauged by the coupling length $L_c = \lambda/[2\mathrm{Re}(n_{even} - n_{odd})]$, where n_{even} and n_{odd} denote, respectively, the effective refractive indices of even and odd modes. The CMT derived in [45] is limited in lossless waveguides but the result can still be used in lossy waveguides if the difference between the real parts of the effective refractive index is far greater than that between the imaginary parts of the effective refractive index for the two modes [46]. In the proposed SHPW structure, the difference between the imaginary parts is two orders of magnitude smaller than that between the real parts. Therefore, the formulation for calculating the coupling length defined in [45] is adopted in the proposed waveguide. In addition to using L_c, a more intuitive picture to evaluate coupling strength is using the normalized coupling length L_c/L_{ave} [46], which expresses the ratio of the coupling length to the mean propagation length L_{ave} of even and odd modes. This is because the maximum transfer power ρ_{max} from one channel to the other can be formulated as a function of L_c/L_{ave}. If the value of L_c/L_{ave} exceeds 10, ρ_{max} approaches zero, and it is deemed that no coupling occurs between waveguides. To further confirm the accuracy of the L_c obtained from the CMT, we also present the 3D simulations of the directional coupler, illustrating the power evolution along the propagation direction z.

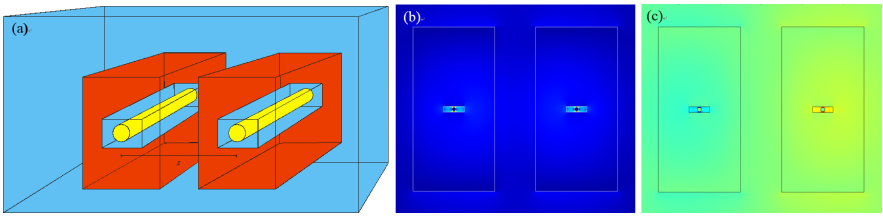

Fig. 7. (a) Schematic of a directional coupler made of two proposed SHPWs, and s is the center-to-center separation distance. Field distributions of E_y for the (a) even and (b) odd modes of the directional coupler with dimensions g = 2 nm, d = 10 nm, w_a = 50 nm, w = 200 nm, h = 400 nm, and s = 0.3 μm.

In this section, we consider three geometries of Si with dimensions of d = 10 nm and w_a = 50 nm to investigate the coupling length of the directional coupler composed of the proposed structures. The corresponding mode characteristics for a single SHPW are listed in Table 2. The values of A_e/A_0 for the three cases are of the same order, approximately 10^{-2}, but the values of Re(n_e) and L_m are much different.

Table 2. Mode Properties for Three Different Silicon Geometries

Mode properties	Re(n_e)	A_e/A_0	L_m (mm)	FOM
I (w = 150 nm, h = 300 nm)	1.58076	1.93×10^{-2}	20.24	1.67×10^5
II (w = 200 nm, h = 400 nm)	2.10765	1.41×10^{-2}	9.77	9.41×10^4
III (w = 250 nm, h = 500 nm)	2.51305	1.62×10^{-2}	11.42	1.03×10^5

For the three cases, the calculated results of Re(n_e) for the even, odd, and single waveguide modes are shown in Fig. 8(a). As the separation distance increases, the values of Re(n_e) for even and odd modes approach those of a single waveguide. The phenomenon shows that the decoupling (no crosstalk) appears when the two waveguides are sufficiently far apart. The degeneracies of the two normal modes for the three conditions occur at different separations. In Fig. 8(a), we note that case I cannot support odd modes that leak into the SiO_2 cladding when the separation is smaller than 0.45 μm. From the results, we see that the decoupled separation evidently depends on the value of Re(n_e). As the value of Re(n_e) increases, the separation achieving no power transfer becomes smaller. The result can be explained by the better confinement for a single SPHW. To quantitatively analyze the coupling strength, L_c/L_{ave} and ρ_{max} versus s are shown in Fig. 8(b). Reasonably, increasing separation distance leads to a monotonic increase in L_c/L_{ave}. If the ratio of L_c/L_{ave} = 10 is

#199173 - $15.00 USD Received 8 Oct 2013; revised 18 Nov 2013; accepted 18 Nov 2013; published 21 Nov 2013

reached, the maximum transfer power reduces to 0.33% relative to input power. This criterion is used in this paper to consider that decoupling has been achieved. For the same separation, L_c/L_{ave} in case III is the largest while in case I it is the smallest. This result is explained by the fact that the coupling strength between two adjacent waveguides depends mainly on the overlap extent of the evanescent tails of the guided modes from each individual waveguide. Case III, with the largest Re(n_e), has a larger field decay rate, in comparison with the other cases, resulting in a weaker coupling between waveguides. For cases II and III, L_c/L_{ave} vary by five orders of magnitude as separation distances are changed from s = 0.4 to 2.0 μm and s = 0.3 to 1.7 μm, respectively. This result indicates that cases II and III provide sufficient flexibility to build various photonic devices. To confirm the accuracy of the L_c obtained from the CMT, we present 3D simulations of the directional coupler.

The 3D calculations in COMSOL use the beam envelopes interface of wave optics module. The electric field can be factored into a slowly varying amplitude factor and a rapidly varying phase factor, and this interface solves for the slowly varying amplitude factor without huge memory requirements. In particular, the module also considers the second-order derivatives to the propagation direction, therefore the accuracy to simulate large-angle propagations is superior to the generally used beam propagation method (BPM) [47] with only considering the first-order derivative. The excitation of the input fields are the even and odd guided modes of the directional coupler and the scattering boundary condition is used to enclose the large enough computational window of 5 μm × 5 μm effectively avoiding the disturbance from the boundary. The degrees of freedom used are 377204 unknowns and the memory are about 30 GB. The computational time is 620 seconds on an *i*7-2600 CPU with eight cores and 3.40 GHz. The energy transfers from the left channel gradually to the right waveguide [see Fig. 7] because of the evanescent coupling between waveguides along the z direction. The black circles [Fig. 8(b)] indicate the results obtained from the 3D simulations, and they are found to be in good agreement with the CMT calculations. The comparisons demonstrate that the CMT is accurate enough to study the proposed SHPW structure.

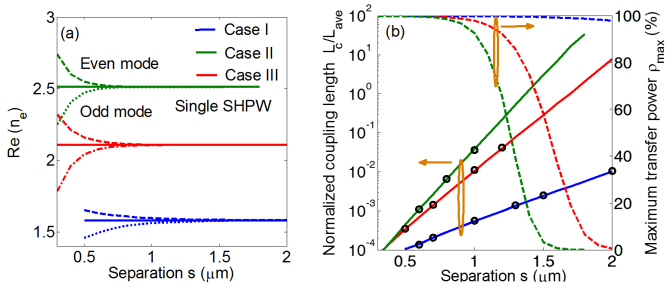

Fig. 8. (a). Real parts of the effective refractive index for even and odd modes of the directional coupler composed of two SHPWs, along with a single SHPW for comparison, and (b) the normalized coupling length L_c/L_{ave} (solid lines) and maximum transfer power ρ_{max} (dashed lines) as functions of separation for three different sizes (see the text for details) of Si. The black circles are the results obtained from 3D simulations.

To design compact photonic components (with strong coupling required), such as switches and multiplexers, the directional coupler based on case III could achieve ρ_{max} = 99.9% at s = 0.26 μm in a coupling length of only L_c = 1.16 μm that is approximately 4000 times smaller than the propagation length. Comparing to the silicon waveguides (L_c = 4.13 μm) and other plasmonic waveguides, such as the double low-index nano-slots [17] (L_c = 93.35 μm), the DLSPPW [48] (L_c = 6.61 μm), and the structures with a metal cap on a silicon-on-insulator rib [49, 50] (L_c > 5 μm) at the separation distance s = 0.4 μm, the proposed structure of case III (L_c = 3.97 μm) shows better compactness than those of other ones. In contrast, by increasing s to 1.65 μm, ρ_{max} is significantly reduced to 0.3% meaning negligible coupling (i.e., L_c/L_{ave} = 10), and it sets the maximum integration scale for realizing photonic

#199173 - $15.00 USD Received 8 Oct 2013; revised 18 Nov 2013; accepted 18 Nov 2013; published 21 Nov 2013

integrated circuits. In comparison with two other structures, a directional coupler composed of two high-refractive-index dielectric slabs with a finite-width insulator metal structure [24] and one composed of two long-range dielectric-loaded surface plasmon polariton waveguides (LR-DLSPPWs) [32] require separations of s = 3.3 μm and s = 5 μm, respectively, to achieve no coupling. The results verify that the proposed SHPW allows higher integration than these other two designs. In contrast, for case I, L_c/L_{ave} varies moderately as s increases, and the coupling strength is still significant even though s reaches 3 μm. Therefore, case I is not suitable for building high-density photonic components.

To observe the energy transfer process, the energy intensity profiles at the middle of the gap along the z direction are shown in Figs. 9(a)–9(c), respectively, for cases I, II, and III, all with s = 0.6 μm. Moreover, the corresponding 3D power evolution of the three cases along the directional coupler are also shown in Figs. 9(d)–9(f). Different from lossless directional couplers composed of two identical waveguides, for directional couplers composed of lossy materials, the power exchange pattern is asymmetric, showing different positions of minimum power in one channel and maximum power in the other channel [Fig. 9]. This is because the even and odd modes experience different metallic absorption during the power transfer process in the directional coupler [51], and the deviation of positions increases as the average attenuation of the two modes increases. Nevertheless, the deviation is slight because the losses of the proposed symmetric SHPW are fairly low. Accordingly, the coupling length based on the minimum power in the through channel [see Figs. 9(a)–9(c)] is very close (the position difference is approximately 0.1 μm) to that based on the maximum power in the cross channel.

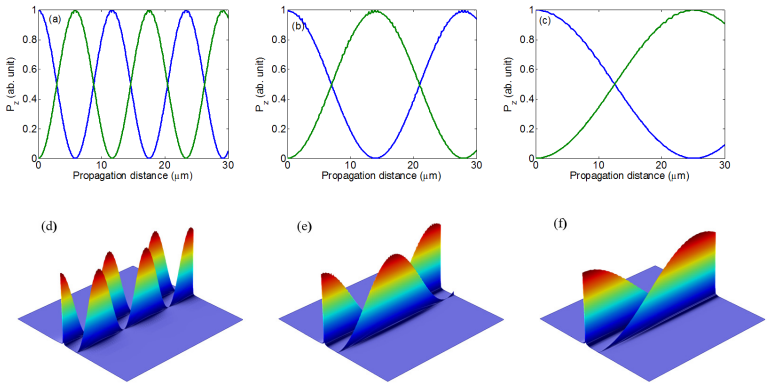

Fig. 9. Poynting vectors P_z for cases (a) I, (b) II, and (c) III for the proposed SHPW for s = 0.6 μm along the propagation direction, and the 3D power evolutions of cases (d) I, (e) II, and (f) III.

To further examine the feasibility of the proposed SHPW in designing the wavelength selective components, we analyze the dependence of the coupling length and the excitation wavelength across the range of λ = 1.4 to 1.65 μm—taking into account material dispersion—for the three cases with separation of s = 0.7 μm. The calculated results are shown in Fig. 10. For case III, the coupling length is L_c = 140.3 μm for wavelength of 1.4 μm and is L_c = 37.7 μm (approximately three times smaller than that at λ = 1.4 μm) for the wavelength of 1.65 μm. The ratios of L_c for λ = 1.4 μm and λ = 1.65 μm are approximately four and two times for the cases II and I, respectively. As the separation increases, the ratio of the coupling lengths for λ = 1.4 μm and λ = 1.65 μm increases substantially. The significant differences in L_c confirm that the proposed SHPW is very promising for the realization of wavelength selective components. Overall, a strong dependence of coupling length on both wavelength and separation makes cases II and III highly promising for realizing a number of plasmonic components.

#199173 - $15.00 USD Received 8 Oct 2013; revised 18 Nov 2013; accepted 18 Nov 2013; published 21 Nov 2013

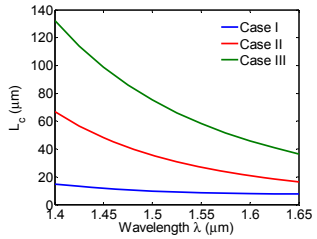

Fig. 10. The coupling length L_c versus excitation wavelength for the three cases (see the text for details) of the proposed SHPW for s = 0.7 μm.

4. Bending loss of the proposed SHPW

For packing compact photonic integrated circuits, maintaining low radiation (bending) loss while transmitting light signals in a sharp bend is another important requirement. To evaluate the bending performance of a 90° bend of the proposed SHPW, the power transmission, T (%), for the three cases are shown versus the bending radius r [depicted in the inset in Fig. 11(a)]. The power transmission is defined as the ratio of the Poynting vector integral at the input plane to that in the output plane. Theoretically, the total loss includes bending loss and propagation loss due to Ohmic absorption. Nevertheless, the calculated transmission is dominated mainly by bending loss due to the ultra-low propagation loss in the proposed SHPW. As a result, the presence of an optimum radius of curvature reported in [52] is not observed in the range of radius considered here. As the radius of curvature increases, T monotonically increases. For case III, the transmission achieves 82.7% at a fairly small bending radius of 0.5 μm, and it continuously increases beyond this radius, reaching 90% at r = 0.8 μm. For case II, r >1.2 μm is required for achieving transmission of 90%. The results demonstrate that cases II and III will be of practical use in constructing highly compact photonic integrated circuits. However, T in case I are approximately 20% to 30%, even when r exceeds 3 μm. Comparing to the bending losses [black circles in Fig. 11(a)] of a silicon waveguide, the proposed SHPW shows the comparable guiding ability to the silicon waveguide. However, the application areas of the plasmonic waveguides are different from that of pure dielectric waveguides because of the extremely enhanced field and the easy surface functionalization of metals by biological molecules [53]. Accordingly, it should be reasonable to compare the performances of the proposed SHPW to that of other plasmonic waveguides. Also, the 3D power evolution of cases I, II, and III are shown in Figs. 11(b)–11(d), respectively, with r = 1.0 μm. The calculated powers for each of the output planes in cases I, II, and III are 25.9%, 87.9%, and 95.8%, respectively; furthermore, large radiation loss leaking out of the waveguide in case I is clearly seen [Fig. 11(b)]. In contrast, most of the mode energy in cases II and III are carried in the waveguides, resulting in small radiation loss.

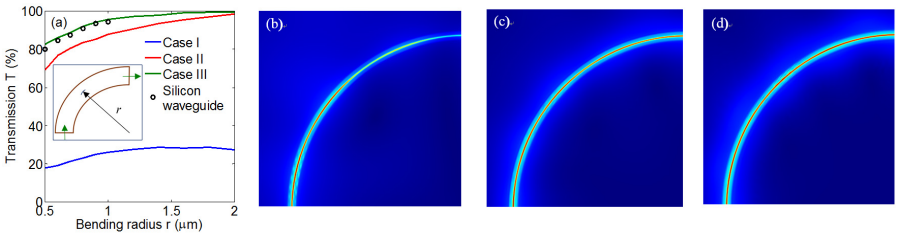

Fig. 11. (a) The power transmission (%) versus the bending radius of the three cases. The power evolution of cases (b) I, (c) II, and (d) III at radius of curvature r = 1 μm.

Furthermore, the spectral response of transmission at r = 0.7 μm in case II is analyzed and the calculated result is shown in Fig. 11. The power transmission shows monotonic decrease as wavelength increases over the wavelength range of 1.4 to 1.65 μm; this is to be expected

#199173 - $15.00 USD Received 8 Oct 2013; revised 18 Nov 2013; accepted 18 Nov 2013; published 21 Nov 2013

because more of the mode distribution extends out of the gap region, resulting in larger radiation loss. In Fig. 12, we observe that the variation of transmission is moderate as the wavelength changes. This means that the power flow based on the present SHPW through a 90° sharp bend over a wide range of wavelength is rather uniform, which is beneficial for designing wavelength multiplexers.

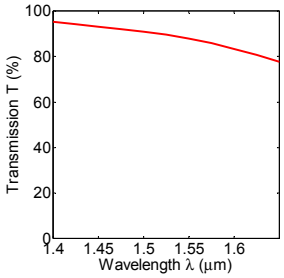

Fig. 12. The power transmission (%) versus excitation wavelength for case II, for radius of curvature $r = 1$ μm.

5. Conclusion

We have proposed a symmetric plasmonic waveguide consisting of a cylindrical metal nanowire surrounded by low-index SiO_2 and high-index Si covered with SiO_2. We have shown that the longitudinal electric field, responsible for the metal absorptions, is minimized. The proposed structure could propagate a millimeter-scale distance with normalized mode areas on the order of approximately 10^{-2} at telecom wavelengths. As a result, the high FOM ($\sim 10^5$), which is one order of magnitude larger than that of other structures, can be achieved. In addition, the coupling strength of a directional coupler composed of two proposed waveguides was discussed, showing that the coupling length can be tuned over a range of five orders of magnitude for waveguide separations between 0.3 and 1.7 μm. To construct compact photonic devices, e.g., for switches and multiplexers, a separation of 0.26 μm could achieve a maximum transfer power of 99.9% in a coupling length of only 1.16 μm (~4000 times smaller than the propagation length). In contrast, increasing the separation to 1.65 μm totally prevents coupling from adjacent waveguides, allowing for a high-density integration of photonic devices. Also, the power transmission of a 90° bend, based on the proposed structure, was studied and showed >80% transmission for a small radius of curvature, 0.5 μm. Moreover, a strong wavelength dependence, across the range of 1.4 to 1.65 μm, on the coupling length shows that the proposed structure is also promising for realizing wavelength-selective components. From our analysis, we believe that the proposed plasmonic waveguide is of practical interest not only to build long-range plasmonic circuit interconnects but also to realize high-density and compact photonic integrated circuits.

Acknowledgments

The author would like to thank the National Science Council of Taiwan for financially supporting this research under Contract No. NSC 102-2112-M-005-008-MY3.

#199173 - $15.00 USD Received 8 Oct 2013; revised 18 Nov 2013; accepted 18 Nov 2013; published 21 Nov 2013